Laboratory Demonstration of Electronic Polarization Basis Rotation

A.J. Gasiewski and D.B. Kunkee

School of Electrical Engineering
Georgia Institute of Technology
Atlanta, GA 30332-0250

Abstract-A hardware and software technique for rotation of the polarization basis of a dual orthogonal-linearly polarized radiometer is discussed. The technique requires precise measurement of the two orthogonal-mode antenna temperatures along with cross-correlation of the two mode amplitudes (the first three Stokes parameters). An innovative polarized blackbody load was developed for accurate calibration of the cross-correlating channel. Using 90-GHz near-Brewster angle observations of a polarizing water surface, rotation of the antenna's polarization basis by a matrix transformation was performed. The experimental results demonstrate the viability of Electronic Polarization Basis Rotation (EPBR) and suggest practical calibration schemes for full-polarization radiometers. Applications of EBPR include mechanically-scanned polarization-sensitive imaging radiometers.

1. Introduction

In passive microwave remote sensing, it is often desirable to construct precision radiometers with dual orthogonal-linear polarization sensitivity. For example, in Earth remote sensing, the additional information obtained by observing both vertically and horizontally polarized brightness temperatures can be used to improve estimates of rainfall, water vapor, and ocean surface winds and to enhance the detectability of sea ice. Orthogonal-polarized information can also be used to enhance passive microwave imagery for surveillance or tracking purposes.

Perhaps the simplest design for a dual-polarization imaging radiometer consists of a dual orthogonal-linearly polarized feedhorn and a mechanically-scanned reflector. The reflector can either be a flat mirror or a shaped antenna. Two commonly used designs are the conical-scanner and cross-track scanner, as found on many spaceborne passive microwave meteorological sensors (e.g., SMMR: Scanning Multichannel Microwave Radiometer, AMSU: Advanced Microwave Sounding Unit and SSM/I: Special Sensor Microwave/Imager). It is desirable from a mechanical standpoint to rigidly fix the radiometer and feedhorn to the host craft and to scan only the reflector. Unfortunately, if the feedhorn remains stationary, the polarization basis of the instrument will rotate throughout the scan. This produces an undesirable skew of the instrument's polarization basis with respect to the scene's polarization basis. The resulting "polarization mixing" caused significant difficulty in interpreting dual-polarization imagery from the SMMR instrument. To circumvent the problem, the conically-scanned SSM/I imager was built with the feedhorn and associated receiver electronics as part of an assembly that rotated in synchronism with the scanning mirror. However, this is both cumbersome and expensive as it requires space-qualified bearings and slip rings and increased rotational inertia.

We discuss here a practical technique to provide polarization basis coincidence using a rigidly-fixed polarization-correlating radiometer with a dual-polarization feedhorn. The technique, called Electronic Polarization Basis Rotation (EPBR) [1], consists of measuring the first three feedhorn Stokes parameters (T_{fA}, T_{fB}, and T_{fU}), then subsequently rotating the polarization basis to a desired basis by a matrix transformation.

As an example, consider passive Earth remote sensing from space. Here, the desired polarization basis is the natural basis (v, h) defined by the local vertical and horizontal directions. The linear transformation of brightness temperatures $\overline{T}$ defined in this basis to the feedhorn temperatures $\overline{T}_f$ defined in the instrument's polarization basis is:

$$\begin{pmatrix} T_{fA} \\ T_{fB} \\ T_{fU} \end{pmatrix} = \begin{bmatrix} \cos^2\phi & \sin^2\phi & \frac{1}{2}\sin 2\phi \\ \sin^2\phi & \cos^2\phi & -\frac{1}{2}\sin 2\phi \\ -\sin 2\phi & \sin 2\phi & \cos 2\phi \end{bmatrix} \begin{pmatrix} T_v \\ T_h \\ T_U \end{pmatrix}$$
$$= \overline{\overline{U}}(\phi) \cdot \overline{T} \qquad (1)$$

where $T_{fU} = Re\langle E_A E_B^* \rangle$ is the cross-correlation between the two orthogonal linearly polarized feedhorn modes (A and B). The angle ϕ is the basis rotation angle, and is a function of the scan mirror angle. Using EPBR, the brightness temperatures in the natural basis are found from the brightness temperatures in the feedhorn basis by inversion of Eq. 1:

$$\overline{T} = \overline{\overline{U}}(-\phi) \cdot \overline{T}_f \qquad (2)$$

A practical implementation of EBPR was proposed by Gasiewski [2], whose scheme included a polarizationcorrelating radiometer and polarized blackbody load. In this paper, we discuss the operation and calibration of the radiometer, focussing on the following issues: (1) hardware implementations of the T_{fU}-channel exhibiting acceptably small crosstalk and instrument noise, (2) calibration of radiometric channels, particularly T_{fU}, (3) laboratory demonstration of EPBR using Eq. 2, and (4) potentially useful applications of the third and fourth Stokes parameters (T_U and T_V) in Earth remote sensing.

IF1

CH3141-9/92/0000-0329$01.00 © 1992 IEEE

2. Hardware

The radiometer (Fig. 1) is a 91.65-GHz dual orthogonal-linearly polarized unit with three outputs: one for each of the two orthogonal feedhorn polarizations (v_A and v_B) and a third cross-correlation channel (v_U). The v_U channel is implemented using an adding correlator and a post-detection summing circuit. The summing circuit removes the relatively large signals caused by the squaring of the IF voltages in each of the channels A and B. Dicke-switching is used to reduce the effects of receiver gain and offset fluctuations. The phase difference of the LO signal at each mixer was nulled using an adjustable phase shifter, represented by $\Delta\varphi$. In addition the path length of the two IF signals was equalized to within one correlation length $l_c = v_p/W \sim 5$ cm, where $v_p \sim 10^8$ m/sec is the IF transmission line phase velocity, and $W = 2$ GHz is the IF bandwidth. The feedhorn cross polarization rejection was approximately 15 dB. The noise temperatures T_{SYS} of the two receivers were estimated to be approximately 1200 and 3600 K, respectively.

The three signals are linearly related to the first three feedhorn Stokes' parameters:

$$\begin{aligned}\overline{v} &= \begin{bmatrix} g_{AA} & g_{AB} & g_{AU} \\ g_{BA} & g_{BB} & g_{BU} \\ g_{UA} & g_{UB} & g_{UU} \end{bmatrix} \cdot \begin{pmatrix} T_{fA} \\ T_{fB} \\ T_{fU} \end{pmatrix} + \begin{pmatrix} o_A \\ o_B \\ o_U \end{pmatrix} + \overline{n}_v \\ &= \overline{\overline{g}}\,\overline{T}_f + \overline{o} + \overline{n}_v \end{aligned} \quad (3)$$

where $\overline{v} = \begin{pmatrix} v_A \\ v_B \\ v_U \end{pmatrix}$ is the video output voltage vector, $\overline{\overline{g}}$ and $\overline{o}$ are the radiometer gain and offset parameters, and $\overline{n}_v$ is the instrument noise referred to the video outputs.

Interchannel crosstalk, manifested by small but nonzero diagonal elements in $\overline{\overline{g}}$ is practically unavoidable. In above radiometer, this was attributed to: (1) unavoidable misalignment of the summing circuit, and (2) relatively weak polarization isolation in the feedhorn. The first of these primarily causes the off-diagonal elements g_{UA} and g_{UB} to be nonzero, while the second causes g_{AA} and g_{BB} to be nonzero. Although the magnitudes of the off-diagonal terms are hardware-specific, they are expected to be significant in nearly all hardware implementations. Provided that the total IF and video gains associated with the power splitters, square-law detectors, and integrators are matched to within ~ 0.5 dB, the gain parameters g_{UA} and g_{UB} are small compared to g_{UU} and $\overline{n}_v$ is uncorrelated among channels. Balancing was accomplished by video and IF component matching, gain adjustment, and thermal stabilization.

Upon calibration, the feedhorn brightness temperature measurements (denoted by $\hat{\cdot}$) are subsequently computed from $\overline{v}$:

$$\begin{aligned}\hat{\overline{T}}_f &= \overline{\overline{g}}^{-1}(\overline{v} - \overline{o}) \\ &= \overline{T}_f + \overline{n}_T \end{aligned} \quad (4)$$

where $\overline{n}_T = \overline{\overline{g}}^{-1}\,\overline{n}_v$. Since $\overline{\overline{g}}$ is nearly diagonal, $\overline{n}_T$ has nearly diagonal covariance:

$$\overline{\overline{R}}_{\overline{n}_T\,\overline{n}_T} = \langle \overline{n}_T \overline{n}_T^t \rangle \approx \begin{bmatrix} \sigma_{TA}^2 & 0 & 0 \\ 0 & \sigma_{TB}^2 & 0 \\ 0 & 0 & \sigma_{TU}^2 \end{bmatrix} \quad (5)$$

where $(\cdot)^t$ is the transpose operator. The noise standard deviations are:

$$\begin{aligned}\sigma_{TA} &= \frac{2T_{SYS,A}}{\sqrt{W\tau}} \\ \sigma_{TB} &= \frac{2T_{SYS,B}}{\sqrt{W\tau}} \\ \sigma_{TA} &= \frac{2\sqrt{T_{SYS,A}T_{SYS,B}}}{\sqrt{W\tau}} \end{aligned} \quad (6)$$

where τ is the effective integration time and the factor of two results from Dicke switching. For the above system the integration time was chosen so that $\sigma_T < 0.1$ K for all channels.

3. Calibration

The elements of $\overline{\overline{g}}$ and $\overline{o}$ are required to convert the output voltages into feedhorn brightnesses. However, both $\overline{\overline{g}}$ and $\overline{o}$ remain stable only over a time scale of minutes and thus need to be periodically calibrated. This was accomplished using a polarized calibration load (Fig. 2) consisting of two highly-absorbing microwave blackbody absorbers and a polarization-splitting wire grid. One load is cooled to a low kinetic temperature T_{COLD} and the other heated to a high temperature T_{HOT} where $T_{HOT} - T_{COLD} \approx 80$ K. The wire grid combines the two load brightness temperatures into two orthogonal- linear polarizations. The resulting principal brightnesses T_1 and T_2 are precisely calculable from measurements of T_{HOT} and T_{COLD}, along with a-priori knowledge of the wire grid transmission and reflection coefficients [3], the load emission and bistatic scattering properties, and the load background brightness temperatures. (For ideal loads and an ideal wire grid $T_1 = T_{COLD}$ and $T_2 = T_{HOT}$.)

By rotating the load around the feedhorn axis, the radiometer feedhorn is illuminated by a variety of precisely known Stokes vectors. The resulting voltages are related to the load temperatures by:

$$\begin{pmatrix} v_A(\alpha) \\ v_B(\alpha) \\ v_U(\alpha) \end{pmatrix} = \overline{n}_v + \begin{bmatrix} g_{AA}(T_1\cos^2\alpha + T_2\sin^2\alpha) + g_{AB}(T_1\sin^2\alpha + T_2\cos^2\alpha) + \\ \qquad g_{AU}(T_2 - T_1)\sin 2\alpha \\ g_{BA}(T_1\cos^2\alpha + T_2\sin^2\alpha) + g_{BB}(T_1\sin^2\alpha + T_2\cos^2\alpha) + \\ \qquad g_{BU}(T_2 - T_1)\sin 2\alpha \\ g_{UA}(T_1\cos^2\alpha + T_2\sin^2\alpha) + g_{UB}(T_1\sin^2\alpha + T_2\cos^2\alpha) + \\ \qquad g_{UU}(T_2 - T_1)\sin 2\alpha \end{bmatrix}$$

where α is the load orientation angle. The effective integration time for calibration was increased so that the instrument noise was negligible. To calibrate, voltage measurements were made at several values of α, resulting in a gain/offset observation matrix $\overline{\overline{C}}$ for each channel. For example, for the U-channel:

$$\begin{pmatrix} v_U(\alpha_1) \\ v_U(\alpha_2) \\ \vdots \\ v_U(\alpha_m) \end{pmatrix} = \overline{\overline{C}}_U \cdot \begin{pmatrix} g_{UA} \\ g_{UB} \\ g_{UU} \\ o_U \end{pmatrix} \quad (7)$$

However, unambiguous inversion of Eq. 7 required that $\overline{\overline{C}}_U$ be full row rank. This was insured for all channels by three

measurements at angles $\alpha = 0, 45$ and 90^o and an additional measurement of an unpolarized calibration load with brightness T_{UP}. Thus:

$$\begin{pmatrix} v_U(\alpha=0^o) \\ v_U(\alpha=45^o) \\ v_U(\alpha=90^o) \\ v_U(\mathrm{UP}) \end{pmatrix} = \begin{bmatrix} T_2 & T_1 & 0 & 1 \\ \frac{T_2+T_1}{2} & \frac{T_2+T_1}{2} & \frac{T_2-T_1}{2} & 1 \\ T_1 & T_2 & 0 & 1 \\ T_{UP} & T_{UP} & 0 & 1 \end{bmatrix} \cdot \begin{pmatrix} g_{UA} \\ g_{UB} \\ g_{UU} \\ o_U \end{pmatrix}$$

$$= \overline{\overline{C}}_U \cdot \begin{pmatrix} g_{UA} \\ g_{UB} \\ g_{UU} \\ o_U \end{pmatrix} \quad (8)$$

The inverse $\overline{\overline{C}}_U^{-1}$ exists provided that $T_2 \neq T_1$. The A and B channels are similarly calibrated.

In practice, several simple variations on the above scheme can provide full row-rank gain/offset observations matrices for all three channels. For example, the unpolarized load measurement can be accomplished by either removing the wire grid or directing the feed toward another load via a splash plate. On a satellite, cold space can be viewed. Alternately, a design consisting of a semi-cylindrical cold load, rotating wire grid, and cold space can yield an invertable matrix $\overline{\overline{C}}$. This design requires only a single low-mass moving element.

4. Laboratory Demonstration

Near Brewster-angle observations of a fresh water surface made using the polarization correlating radiometer and a conically-scanned mirror were performed to demonstrate the EPBR technique and radiometer calibration scheme. The experiment (Fig. 3) consisted of a conical scan of a calm water surface at close-range and an incident angle of 65^o with respect to vertical. The measurements were made outdoors in clear-air, thus the background brightness was relatively cold and unpolarized.

Calculations using a planar-stratified radiative transfer model [4] were performed to determine the predicted upwelling brightness temperatures. The water reflectivity was computed using the Fresnel relations and the Debye model for the dielectric constant [5] along with the measured water temperature. Under these conditions, $\hat{\overline{T}}$ was computed to be (258.5,132.5,0) K. The corresponding degree of polarization of the upwelling radiation field is 0.32, indicating moderate polarization.

Upon determination of $\overline{\overline{g}}$ and $\overline{o}$ by inversion of Eq. 8 brightness temperatures in the feedhorn and natural bases were found by:

$$\hat{\overline{T}}_f(\phi) = \overline{\overline{g}}^{-1}(\overline{v} - \overline{o})$$
$$\hat{\overline{T}} = \overline{\overline{U}}(-\phi) \cdot \hat{\overline{T}}_f(\phi) \quad (9)$$

where ϕ is the basis rotation angle. As illustrated in Fig. 4, $\hat{\overline{T}}_f$ varies significantly througout the scan due to polarization mixing. However, the measured values of T_v and T_h track the predicted values (solid straight lines) well. A relatively small systematic discrepancy of less than ~ 7 K is attributed to mechanical misalignment of the scan mirror with the feedhorn axis and bias in the radiative transfer calculation caused by uncertainties in the assumed atmospheric state. Note that the measured value of T_U is essentially zero in the natural basis, as expected.

5. Discussion

The EPBR demonstration illustrates the capability to unambiguously recover vertical and horizontal brightnesses with a mechanically-scanned imager and fixed-feed polarization-correlating radiometer. Applications of EPBR include polarized radiometric imaging systems, particularly cross-track and conical scanners for space- or airborne passive microwave imaging.

It is noted that calibration of a polarization-correlating radiometer requires a sightly more sophisticated scheme than the familiar two-blackbody (hot and cold load) technique. The familiar technique is applicable for calibration of single- and dual-polarization radiometers where only two parameters per channel (a gain and offset) need to be determined. However, determining the three gain parameters (including crosstalk) and one offset parameter of the $U-$channel on a polarization-correlating radiometer requires a set of feedhorn Stokes vectors that will allow these four parameters to unambiguously measured. The polarized blackbody load is a simple passive structure for this purpose. Moreover, the broadband nature of the components (wire grid and blackbody absorbers) makes the polarized load well-suited for calibration of wideband multichannel radiometers.

While the usefullness of vertically and horizontally polarized brightness information in passive Earth remote sensing is well known (e.g., [6]), comparatively few studies of the potential uses of the third and fourth Stokes parameters have been made. However, there is growing interest in passive microwave remote sensing of terrestrial surface parameters using full polarization measurements [7]. For example, recent simulations suggest values of T_U as high as 50 K for certain periodic surfaces [8]. Using a calibrated polarization radiometer, measured values of T_U in the natural basis are readily obtained as a by-product of EBPR.

Although astronomical radio sources are often circularly polarized, measurements of the fourth Stokes parameter $T_V = Im\langle E_V E_H^* \rangle$ are not generally thought to be useful for remote sensing of the terrestrial troposphere or lower stratosphere. However, upper stratospheric and mesospheric Zeeman splitting by the Earth's magnetic field causes significant differences between left- and right circularly polarized microwave brightness temperatures [9]. Consequently, T_V is of great interest in temperature sounding at altitudes from 40 to 75 km. Since T_V is invariant under basis rotation (i.e., $T_{fV} = T_V$), it is unaffected by mechanical scanning mirrors, and thus does not benefit from EPBR. However, by simply adding $\pm 90^o$ to the LO phase shift φ of a calibrated polarization correlation radiometer T_V can be measured with the same accuracy as T_U. Here, the T_V measurement accuracy is facilitated by prior calibration of the T_{fU}-channel using the polarized blackbody load. Thus, the capability to accurately measure both T_U and T_V along with T_v and T_h is an indirect but potentially useful capability of EBPR hardware.

Acknowledgements-This work has been supported by the Georgia Institute of Technology and NASA grant NAG 8-829. The authors also thank the NASA Goddard Space Flight Center for furnishing critical radiometric hardware.

References

[1] Parks, G.S., T.C. Fraschetti, D.C. Miller, "Microwave Precipitation Radiometer", Jet Propulsion Laboratory Study Report JPL D-5397, May 1, 1988.

[2] Gasiewski, A.J. "A Technique for Measuring Vertically and Horizontally Polarized Brightness Temperatures Using Electronic Polarization Basis Rotation", Proceedings of the 1990 IEEE International Geoscience and Remote Sensing Symposium (IGARSS), pp. 1569-1572, May, 1990.

[3] Chambers, W.G., T.J. Parker, and A.E. Costley, Free-standing Fine-Wire Grids for Use in Millimeter- and Submillimeter-Wave Spectroscopy, in *Infrared and Millimeter Waves*, K.J. Button (ed.), Vol. 16, pp. 77-106, 1986.

[4] Gasiewski, A.J., and D.H. Staelin, "Numerical Modelling of Passive Microwave O_2 Observations Over Precipitation", *Radio Sci.*, vol. 25, no. 3, pp. 217-235, 1990.

[5] Klein, L.A., and C.T. Swift, "An Improved Model for the Dielectric Constant of Sea Water at Microwave Frequencies", *IEEE Trans. Ant. Prop.*, vol. AP-25, pp. 104-111, 1977.

[6] Adler, R.F., R.A. Mack, N. Prasad, H.-Y.M. Yeh, and I.M. Hakkarinen, "Aircraft Microwave Observations and Simulations of Deep Convection from 18-183 GHz. Part I: Observations", *J. Ocean. Atm. Tech.*, vol. 7, pp. 377-391, June, 1990.

[7] Kong, J.A., "Theoretical Modelling for Passive Remote Sensing of Earth Terrain", Proceedings of the Specialist Meeting Microwave Radiometry and Remote Sensing, Boulder, CO, Jan. 14-16, 1992.

[8] Veysoglu, M.E., "Polarimetric Passive Remote Sensing of Periodic Surfaces and Anisotropic Media", S.M. Thesis, Department of Electrical Engineering and Computer Science, Massachusetts Institute of Technology, Cambridge, MA, 1991.

[9] Rosenkranz, P.W., and D.H. Staelin, "Polarized Thermal Microwave Emission from Oxygen in the Mesosphere", Radio Science, vol. 23, pp. 721-729, Sept-Oct, 1988.

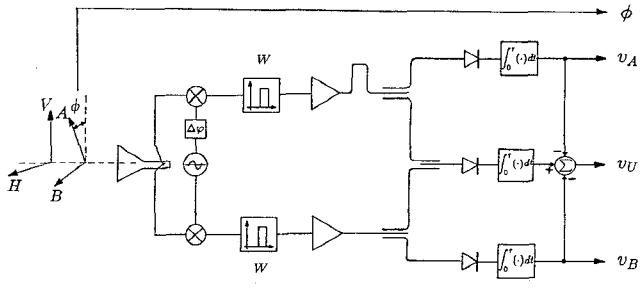

Figure 1: Block diagram of the 3-channel (T_A, T_U and T_B) polarization correlation radiometer.

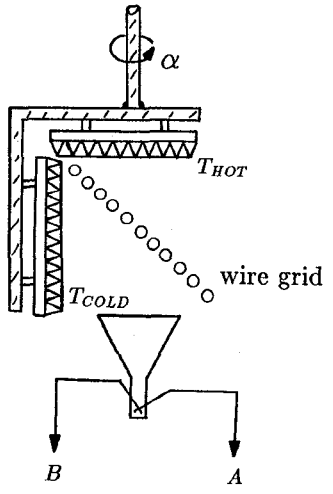

Figure 2: Polarized blackbody calibration load.

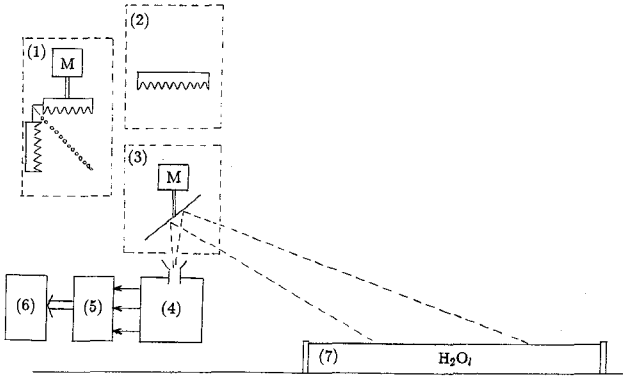

Figure 3: Experiment for demonstrating EPBR: (1) polarized blackbody load, (2) unpolarized load, (3) scanning mirror, (4) polarization correlating radiometer, (5) A/D converters, (6) computer, and (7) water surface.

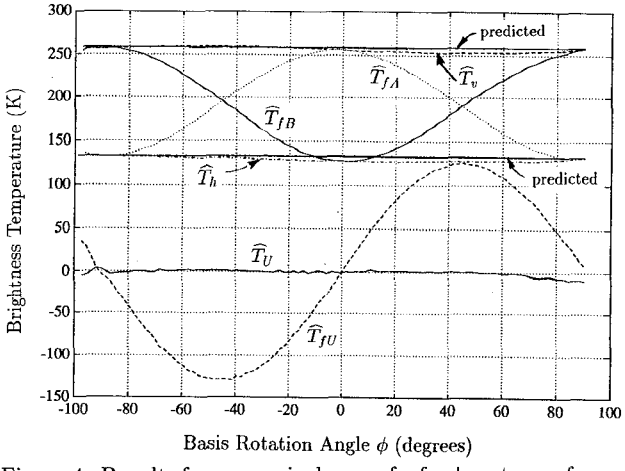

Figure 4: Results from a conical scan of a fresh water surface. The measured feedhorn brightnesses are $\widehat{T}_{fA}$, $\widehat{T}_{fU}$ and $\widehat{T}_{fB}$; measured brightnesses in the Earth's $v-h$ basis are $\widehat{T}_v$, $\widehat{T}_h$ and $\widehat{T}_U$. The solid heavy lines are predicted values of T_v and T_h.